J. Mech. Phys. Solids 208 (2026) 106468

Contents lists available at ScienceDirect

Journal of the Mechanics and Physics of Solids

journal homepage: www.elsevier.com/locate/jmps

A probabilistic buckling model for hemispherical shells with non-interacting localized defects

Zheren Baizhikova [a], Uba K. Ubamanyu [b], Fani Derveni [b,c], Roberto Ballarini [a], Pedro M. Reis [b], Jia-Liang Le [d,*]

[a] Department of Civil and Environmental Engineering, University of Houston, United States
[b] Flexible Structures Laboratory, Institute of Mechanical Engineering, Ecole Polytechnique Federale de Lausanne, Switzerland
[c] Scalable MetaStructures Laboratory, School of Civil and Environmental Engineering, Cornell University, United States
[d] Department of Civil, Environmental, and Geo- Engineering, University of Minnesota, United States

ARTICLE INFO

Keywords:
Shell buckling
Knockdown factor
Probability distribution
Weakest-link model
Statistical size effect
Stochastic simulation

ABSTRACT

This paper presents a combined computational and analytical investigation on the probability distribution of the knockdown factor of hemispherical shells containing multiple non-interacting localized geometrical defects. In the analytical model, the statistics of the knockdown factor for shells with a single defect are explicitly linked to the statistics of the defect amplitude. The model is then extended to shells with multiple non-interacting defects of random amplitudes through a finite weakest-link formulation, which predicts how the mean and coefficient of variation of the knockdown factor depend on the number of defects on the shell surface. The results of extreme value statistics are further used to derive the limiting form of the knockdown-factor distribution. The analytical investigation is accompanied by a series of stochastic finite element (SFE) simulations of hemispherical shells of different dimensions and with different sizes of the zone containing the defects. The analytical model is shown to be in excellent agreement with the simulation results. The main outcome of the analytical model is a statistical size effect on the knockdown factor, governed by the dimensionless radius, for shells containing the maximum possible number of non-interacting defects. A similar size effect has recently been reported for hemispherical shells with continuous random imperfect surfaces. Together, these results offer a new perspective on the universal statistical role of the dimensionless radius in governing the buckling behavior of geometrically imperfect hemispherical shells.

1. Introduction

Reliability-based design of a realistic structure hinges on an understanding of the stochastic nature of its potential failure mechanisms; the uncertainty associated with the structure's response to mechanical loads stems from the inherent randomness of both its resistance and the loads (Ang and Tang, 1984; Haldar and Mahadevan, 2000). While available databases can provide valuable information about the statistics of the loads associated with different types of applications, characterizing the probability distribution of structural resistance requires a mechanistic model formulated within a probabilistic framework. The development of such models for engineering structures susceptible to various failure mechanisms has drawn significant attention within the mechanics

* corresponding author.
E-mail addresses: zbaizhik@cougarnet.uh.edu (Z. Baizhikova), kanthasamy.ubamanyu@epfl.ch (U.K. Ubamanyu), fani.derveni@cornell.edu (F. Derveni), rballari@central.uh.edu (R. Ballarini), pedro.reis@epfl.ch (P.M. Reis), jle@umn.edu (J.-L. Le).

https://doi.org/10.1016/j.jmps.2025.106468
Received 20 October 2025; Received in revised form 1 December 2025; Accepted 1 December 2025
Available online 3 December 2025

community, e.g. (Weibull, 1939; Daniels, 1945; Harlow and Phoenix, 1978; Bažant and Le, 2017; Le, 2020). This includes renewed and growing interest in the development of stochastic models for characterizing the buckling resistance of thin-walled structures that are ubiquitous in civil, aeronautical, nuclear, naval, and biomedical engineering applications (Amazigo, 1969; Elishakoff, 2000; Lee et al., 2016; Wang et al., 2022; Derveni et al., 2023b; Baizhikova et al., 2024).

Consider the illustrative example of a thin-walled spherical shell subjected to uniform pressure. The pressure required to buckle it is highly sensitive to the size, shape, and distribution of geometric imperfections introduced during fabrication and/or in service (Tsien, 1942; Homewood et al., 1961; Carlson et al., 1967; Bažant and Cedolin, 1991). Experimental data have shown that imperfections are responsible for a significantly lower critical pressure than the theoretical value derived for a shell of perfect geometry (Kaplan and Fung, 1954; Carlson et al., 1967; Weingarten et al., 1968; Lee et al., 2016; Derveni et al., 2023b). In addition, the data exhibit considerable degrees of statistical variability, whose quantification is essential for designing thin shell structures that require a tolerable failure probability. The imperfection sensitivity implies that the randomness in buckling resistance is intimately related to the inherent randomness in the size, shape, and distribution of geometric imperfections. The importance of understanding this intricate relationship has long been recognized (Bolotin, 1962; Fraser and Budiansky, 1969; Elishakoff and Cai, 1994; Elishakoff, 2000). Earlier works include Amazigo's study of the stochastic buckling behavior of long cylindrical shells with random, axisymmetric imperfections using the modified truncated hierarchy technique (Amazigo, 1969). With the significant advances in the theory of stochastic processes and computational mechanics, numerical models have become the major tool for investigating the stochastic buckling behavior of shells with geometrically imperfect shapes. Elishakoff applied the Monte Carlo method to study the reliability of axially compressed cylindrical shells with nonsymmetric imperfections (Elishakoff and Arbocz, 1985). In recent studies, the full-scale SFE method was applied to simulate the probability distribution of the pressure required to buckle cylindrical and hemispherical shells with randomly distributed initial geometrical imperfections (Wang et al., 2022; Derveni et al., 2023b; Baizhikova et al., 2024).

Monte Carlo simulation has provided insights into the stochastic buckling behavior of thin-walled structures. However, its high computational cost renders it unfeasible for predicting the design buckling pressure corresponding to a very low failure probability. To sample the region within which the probability of failure is on the order of one in a million would require tens of millions of simulations (Haldar and Mahadevan, 2000). In this regard, analytical modeling of the cumulative distribution function (CDF) must play a pivotal role in reliability-based design. Derveni *et al.* investigated the buckling behavior of spherical shells containing a random distribution of discrete dimple defects and showed that the CDF of buckling pressure could be fitted by the three-parameter Weibull distribution (Derveni et al., 2023b), thus suggesting the applicability of the extreme value statistics to shell buckling.

A recent study by Baizhikova *et al.* proposed a finite weakest-link model for the statistics of buckling resistance of shells whose shape deviated from that of their nominal hemispherical shape, and validated it through SFE simulations that considered different combinations of geometric parameters (Baizhikova et al., 2024). The model shows that, for shells containing a continuous spatial distribution of geometric imperfections, the functional form of the CDF of buckling pressure varies with the dimensionless radius R/t (R and t denote the shell radius and thickness, respectively). As R/t becomes sufficiently large, the buckling pressure asymptotically approaches the three-parameter Weibull distribution. It is well known that the shell radius and thickness mechanistically govern the buckling pressure by setting the characteristic length scale ($\propto \sqrt{Rt}$) of the buckling mode (Hutchinson, 1967; Derveni et al., 2023a). The finite weakest-link model developed in Baizhikova et al. (2024) revealed that, beyond its mechanistic role in buckling analysis, R/t also has a statistical effect on the mean buckling pressure.

The success of the finite weakest-link model is attributed to the fact that buckling of hemispherical shells with geometric imperfections is triggered by localized buckling (Von Kármán and Tsien, 1939; Audoly and Hutchinson, 2020; Derveni et al., 2023b; Baizhikova et al., 2024). This suggests that the buckling pressure is dictated by the minimum value of the critical pressures corresponding to the formation of a buckling zone at all possible locations on their surface. This conjecture has recently been validated through a systematic computational study (Derveni et al., 2025), which demonstrated that the buckling pressure of the shell is governed by the "weakest spot" (the region with the most severe imperfection). Consequently, the CDF of buckling pressure must follow the statistics of the weakest-link type, which represents a general mathematical framework for localization-induced failure phenomena (Le, 2024). Despite these recent advances in probabilistic modeling of buckling in hemispherical shells, an explicit analytical relationship between the randomness of geometric features defining initial imperfections and buckling pressure statistics remains elusive. Such a relationship is critically important for reliability-based design, where structures must be engineered to ensure extremely low failure probabilities, typically on the order of 10^{-6} or less (Bažant and Le, 2017). Since neither experimentation nor numerical simulations can probe the far-left tail of the CDF of buckling pressure, analytical models become indispensable. Recent studies have shown, however, that obtaining such an analytical relationship is extremely challenging when the imperfect geometry is modeled as a continuous random field (Baizhikova et al., 2024).

Here, we derive such a relationship for hemispherical shells containing randomly distributed non-interacting dimple-like defects, where the defects are spaced sufficiently far apart so that the buckling pressure is independent of the defect-defect interactions (Derveni et al., 2023a). Through this relationship, we obtain an analytical model of the dependence of the CDF of buckling pressure on the number of defects, which is validated through a set of SFE simulations. The analytical model directly predicts the statistical size effect on the buckling pressure, governed by the dimensionless radius, for shells containing the maximum possible number of non-interacting defects.

Our paper is organized as follows: Section 2 presents a finite weakest-link model of the knockdown factor, defined as the buckling pressure normalized with respect to the theoretical buckling pressure of a perfect shell. The model explicitly relates the knockdown factor statistics to the statistics of defect size. Section 3 presents a stochastic computational model for calculating the statistics of knockdown factor. The comparison between the analytical model and the results of stochastic simulations is presented in Section 4,

and the consequent size effect on the statistics of knockdown factor is discussed in Section 5. Finally, in Section 6, we summarize our main findings and discuss opportunities for future work.

2. Analytical model of the probability distribution of knockdown factor

It is customary to represent the critical buckling pressure of a spherical and hemispherical shells, p_c , in terms of the knockdown factor, $\kappa = p_c/p_0$, where p_0 is the theoretical buckling pressure of a geometrically perfect linear elastic spherical shell as determined by linear buckling analysis (Zoelly, 1915):

$$p_0 = \frac{2E}{\sqrt{3(1-\nu^2)}}(t/R)^2, \tag{1}$$

where E = Young's modulus, ν = Poisson's ratio, R = radius of the shell, and t = shell thickness. In this section, we formulate a mathematical model that derives the statistics of κ for hemispherical shells containing non-interacting dimples from the probability distribution of the amplitude of the dimple.

First, we consider a hemispherical shell containing a single dimple-like defect at the pole, whose geometry is assumed in the form of an axisymmetric Gaussian profile:

$$w(\beta) = -\delta\, \mathrm{e}^{-(\beta/\beta_0)^2}, \tag{2}$$

where w is the radial deviation, β is the zenith angle from the center of the defect, δ is the amplitude, and β_0 is the characteristic angular half-width parameter. In line with the literature (Koga and Hoff, 1969; Hutchinson, 2016; Lee et al., 2016; Jiménez et al., 2017), the amplitude of each defect is normalized by the shell thickness, $\bar{\delta} = \delta/t$. Additionally, the defect-width parameter $\lambda_I = [12(1-\nu^2)]^{1/4}\beta_0\sqrt{R/t}$ is introduced to define the characteristic width of the dimple, relating its angular size to the shell's geometric and material properties. The dimensionless amplitude $\bar{\delta}$ is treated as a random variable, whose CDF is denoted by $F_{\bar{\delta}}(x)$, while λ_I is assumed to be deterministic. It has been shown (Derveni et al., 2025) that, for given value of λ_I, the relationship between κ and $\bar{\delta}$ can be approximated empirically by

$$\kappa = g(\bar{\delta}) = \kappa_0 + a\exp(-b\bar{\delta}), \tag{3}$$

where κ_0 = threshold of knockdown factor, and $a,\ b$ = constants. For shells with a small value of R/t, κ_0, a, and b also vary mildly with R/t (Jiménez et al., 2017). As $\bar{\delta}$ approaches zero, the knockdown factor converges to unity for full spherical shells. In contrast, hemispherical shells clamped at their equator exhibit a plateau in the knockdown factor for relatively small values of $\bar{\delta}$ (approximately less than 0.07) due to the boundary-induced buckling modes, as recently shown by Ubamanyu et al. (2025). Eq. 3 does not capture this small-amplitude asymptotic behavior, but this is inconsequential for this study because, for the CDF of $\bar{\delta}$ chosen here, the chance of sampling a very small value of $\bar{\delta}$ is vanishingly small. Furthermore, load-carrying structures need to be designed to have a low failure probability (Ang and Tang, 1984; Haldar and Mahadevan, 2000). Therefore, the design of shells is hinged by the knowledge of the left tail of the probability distribution of knockdown factor (small probability of failure), which, in turn, is governed by the large-amplitude behavior of Eq. 3.

As indicated by Eq. 3, the knockdown factor decreases monotonically with increasing defect amplitude until the threshold κ_0 is reached. Therefore, the CDF of knockdown factor of the shell that contains a single defect with a random amplitude can be expressed by

$$F_{\kappa_1}(\kappa) = \Pr(\kappa_1 \le \kappa) = 1 - F_{\bar{\delta}}[g^{-1}(\kappa)], \tag{4}$$

where $g^{-1}(\kappa) = -b^{-1}\ln\left\{\langle\kappa-\kappa_0\rangle/a\right\}$, and $\langle x\rangle$ = Macaulay brackets = $\max(x,0)$.

Next, we consider a hemispherical shell containing N non-interacting dimple defects, whose random dimensionless amplitudes follow the same CDF $F_{\bar{\delta}}(x)$. A recent study has shown that, for shells containing non-interacting defects, the buckling pressure is governed only by the defect with the largest amplitude (Derveni et al., 2025). Furthermore, we assume that these defects are sufficiently far away from the equator so that their local buckling behavior is unaffected by the boundary conditions along it. These defects therefore behave in the same manner as the one located at the pole. What matters for calculating the probability distribution of the buckling pressure is the statistics of the maximum amplitude, $\bar{\delta}_m$, of N defects. Since these defects are statistically independent, the CDF of $\bar{\delta}_m$ is given by

$$F_{\bar{\delta}_m}(x) = \left[F_{\bar{\delta}}(x)\right]^N, \tag{5}$$

Given that the behavior of the single defect is location independent, Eq. 3 can be used to relate the knockdown factor of the shell to the relative amplitude of the most severe defect. Consequently, the CDF of the knockdown factor κ_N can be written as

$$F_{\kappa_N}(\kappa) = 1 - F_{\bar{\delta}_m}[g^{-1}(\kappa)] = 1 - \left\{F_{\bar{\delta}}[g^{-1}(\kappa)]\right\}^N, \tag{6}$$

which provides an explicit relationship between the statistics of defect amplitude and the statistics of knockdown factor.

An alternative way to understand Eq. 6 is via a weakest-link model. Since the defects are non-interacting, the knockdown factor, κ_i, for an individual defect i, can be calculated by considering that the other $N-1$ defects are absent. The knockdown factor of a shell containing N defects is equal to the minimum value of the N knockdown factors corresponding to N defects, i.e. $\kappa_N = \min\kappa_i$ (i =

$1, \ldots, N$). Since the knockdown factors of all N defects are statistically independent and follow the same distribution function $F_{\kappa_1}(\kappa)$, the joint probability theorem dictates that

$$F_{\kappa_N}(\kappa) = 1 - \left[1 - F_{\kappa_1}(\kappa)\right]^N = 1 - \left\{F_{\bar{\delta}}[g^{-1}(\kappa)]\right\}^N, \tag{7}$$

which recovers Eq. 6.

In the weakest-link model, it is of interest to explore the asymptotic behavior of the function $F_{\kappa_N}(\kappa)$ as $N \to \infty$. Based on Eq. 6, we can derive the function $F_{\kappa_N}(\kappa)$ for large values of N from the probability distribution function, $F_{\bar{\delta}_m}(x)$, of the maximum amplitude of N defects. From Eq. 5, the function $F_{\bar{\delta}_m}(x)$ for large values of N is determined by the extreme right tail of the CDF of $\bar{\delta}$, which is referred to as the domain of attraction in the theory of extreme value statistics (Ang and Tang, 1984; Vanmarcke, 2010). For most, if not all, engineering problems, the probability distribution of $\bar{\delta}_m$ would approach one of three extreme value distributions, namely the Gumbel, Frechet, and Weibull distributions. The characteristics of the domain of attraction that determine the form of function $F_{\bar{\delta}_m}(x)$ can be described by the von Mises conditions (von Mises, 1936; Falk and Marohn, 1993). In this study, we assume that $F_{\bar{\delta}}(x)$ has the following property

$$\lim_{x\to\infty} \frac{\mathrm{d}}{\mathrm{d}x}\left[\frac{1 - F_{\bar{\delta}}(x)}{f_{\bar{\delta}}(x)}\right] = 0, \tag{8}$$

where $f_{\bar{\delta}}(x)$ = probability density function (PDF) of the relative amplitude of a single defect. It has been shown that if Eq. 8 holds true, the extreme value distribution function $F_{\bar{\delta}_m}(x)$ approaches the Gumbel distribution in the limit of large N (Ang and Tang, 1984; Falk and Marohn, 1993):

$$F_{\bar{\delta}_m}(x) \approx \exp\left\{-\exp\left[-\alpha_N(x - \gamma_N)\right]\right\}, \tag{9}$$

where α_N and γ_N are constants. Note that α_N and γ_N could depend on the value of N, and this dependence is governed by the right tail behavior of $F_{\bar{\delta}}(x)$.

Substituting Eq. 9 and $g^{-1}(\kappa)$ into Eq. 6 yields

$$F_{\kappa_N}(\kappa) \approx 1 - \exp\left\{-\frac{\langle \kappa - \kappa_0\rangle^{m_N}}{s_N^{m_N}}\right\} \qquad \text{for a large value of } N, \tag{10}$$

where $m_N = \alpha_N / b$ and $s_N = a\exp(-\gamma_N b)$. Eq. 10 indicates that, for large values of N, the CDF of knockdown factor approaches a three-parameter Weibull distribution as an asymptotic distribution function, where the Weibull modulus m_N and Weibull scaling parameter s_N may depend on N.

It follows from Eq. 6 that the CDF of knockdown factor $F_{\kappa_N}(\kappa)$ can be rewritten as

$$F_{\kappa_N}(\kappa) = 1 - \exp\left\{N \ln F_{\bar{\delta}}[g^{-1}(\kappa)]\right\}, \tag{11}$$

which is valid for all N values. Eq. 11 shows that, for large values of N, the entire CDF of knockdown factor is governed by the behavior of $F_{\bar{\delta}}[g^{-1}(\kappa)]$ as $\kappa \to \kappa_0$. By comparing Eq. 11 and Eq. 10, we obtain this asymptotic behavior of $F_{\bar{\delta}}[g^{-1}(\kappa)]$:

$$F_{\bar{\delta}}[g^{-1}(\kappa)] \approx \exp\left\{-\frac{\langle \kappa - \kappa_0\rangle^{m_N}}{N s_N^{m_N}}\right\} \tag{12}$$

Eq. 12 is now used to determine the left-tail of the CDF of knockdown factor for any value of N, which is essential for reliability-based design of shells. From Eq. 7, the CDF $F_{\kappa_N}(\kappa)$ for the low probability regime can be written as

$$F_{\kappa_N}(\kappa) \approx N F_{\kappa_1}(\kappa) \qquad \text{for } \kappa - \kappa_0 \to 0. \tag{13}$$

Since $F_{\kappa_1}(\kappa) = 1 - F_{\bar{\delta}}[g^{-1}(\kappa)]$, combining Eqs. 12 and 13 yields

$$F_{\kappa_N}(\kappa) \approx \frac{\langle \kappa - \kappa_0\rangle^{m_N}}{s_N^{m_N}} \qquad \text{for } \kappa - \kappa_0 \to 0. \tag{14}$$

This equation indicates that, regardless of the number of defects, the left tail of the CDF of knockdown factor follows a power-law with threshold κ_0.

The foregoing analysis considered shells containing a fixed number of defects. In actual design, the number of defects may not be known prior to the manufacturing of the shell. In a general setting, the number of defects could be treated as a random variable with an assumed distribution function, and the CDF of knockdown factor can be expressed by

$$F_{\kappa}(\kappa) = \int_0^\infty F_{\kappa_N}(\kappa)\phi_N(N)\mathrm{d}N, \tag{15}$$

where $\phi_N(N)$ = PDF of the number of defects. Eq. 15 states that the overall CDF of knockdown factor $F_{\kappa}(\kappa)$ of the shell is equal to the expected value of CDF of knockdown factor with respect to the defect number, denoted by $\mathbb{E}_N[F_{\kappa_N}(\kappa)]$. Following Eq. 6, we can rewrite the CDF of knockdown factor for a given defect number by $\ln\left[1 - F_{\kappa_N}(\kappa)\right] = N \ln\left\{F_{\bar{\delta}}[g^{-1}(\kappa)]\right\}$. By taking the expectation of both sides of the equation and making the approximation $\mathbb{E}_N\left\{\ln\left[1 - F_{\kappa_N}(\kappa)\right]\right\} \approx \ln\left\{1 - \mathbb{E}_N[F_{\kappa_N}(\kappa)]\right\}$, we obtain

$$F_{\kappa}(\kappa) \approx 1 - \left\{F_{\bar{\delta}}[g^{-1}(\kappa)]\right\}^{\bar{N}} \tag{16}$$

where $\bar{N}$ = average number of defects on a shell. As will be shown in Sec. 4.2, when the coefficient of variation (CoV) of defect number is relatively small, Eq. 16 gives essentially the same results as Eq. 15. As indicated by Eq. 16, the probability that the knockdown factor is smaller than a given value increases with increasing $\bar{N}$. Therefore, the mean knockdown factor must decrease as $\bar{N}$ increases. This is commonly known as the statistical size effect (Bažant and Le, 2017; Le, 2024).

In scenarios where the number of defects is unknown, it is conservative to assume that the shell contains the maximum number of defects. It has been shown that, to prevent defect interactions, the minimum center-to-center spacing between two defects is proportional to $\sqrt{Rt}$, a characteristic length scale describing the axisymmetrical buckling mode Derveni et al. (2023a), and therefore the area of the non-interacting zone of a single defect scales as $A_{\text{defect}} \sim Rt$. Since the available surface area of a hemispherical shell is $A_{\text{shell}} = 2\pi R^2$, the maximum number of non-overlapping defects that can be distributed over the hemispherical surface is estimated as

$$\bar{N} \sim \frac{A_{\text{shell}}}{A_{\text{defect}}} \sim \frac{2\pi R^2}{Rt} \sim \frac{R}{t}. \tag{17}$$

Hence, the statistical size effect on the mean knockdown factor is governed by the dimensionless radius R/t. The mean knockdown factor of the shell can then be written as

$$\bar{\kappa} = \kappa_1 \Psi(R/t) \tag{18}$$

where κ_1 = knockdown factor of a shell of the same size but containing only one dimple, and Ψ = function describing the statistical size effect. The behavior of the function $\Psi(R/t)$ will be examined in Section 5 by means of numerical simulations.

Extensive studies have shown that the dimensionless radius R/t governs the mechanics of buckling of shells with a single dimple (Audoly and Hutchinson, 2020; Hutchinson and Thompson, 2018; Lee et al., 2016). Therefore, in general, κ_1 also depends on R/t. Eq. 18 provides a complete description of the combined mechanistic and statistical effects of R/t on the knockdown factor of spherical shells containing non-interacting defects with random amplitudes. A recent study has demonstrated that the same equation can also be applied to spherical shells with a spatially random imperfect surface (Baizhikova et al., 2024).

3. Stochastic finite element simulations

To validate the analytical model proposed in the previous Section, we conducted stochastic finite element (SFE) simulations using the commercial software Abaqus/Standard (v2023). In the computational model, the externally pressurized hemispherical shell was represented by its 3D mid-surface, incorporating a spatial distribution of non-interacting geometric imperfections, following a procedure to seed the imperfections similar to previous work by Derveni *et al.* (Derveni et al., 2023a). The mid-surface of the shell was discretized using four-node, reduced-integration shell elements (S4R); a standard choice that offers a favorable trade-off between computational efficiency and accuracy in capturing the buckling behavior. Our approach builds upon the validated framework developed in earlier studies (Abbasi et al., 2023; Derveni et al., 2023a,b), where numerical predictions were found to be in excellent agreement with experimental observations. Based on these prior validations and a thorough convergence study similar to that performed in Ubamanyu et al. (2025), we adopted a discretization consisting of 120,000 total elements, with 200 shell elements uniformly distributed along the meridional arc from the pole to the equator.

Each imperfection, indexed by the subscript $(\cdot)_i$, with the integer $i \in [1, N]$, where N denotes the total number of defects in a given realization, was introduced into an initially perfect shell geometry as an axisymmetric Gaussian dimple defined in Eq. 2. Following the present analytical model, we fixed the angular width of all defects as $\lambda_I = 1$ as a representative and illustrative choice for convenience and consistency with the previous studies (Derveni et al., 2023b). While it is known that the most detrimental value of λ_I depends on the imperfection amplitude δ_i (Lee et al., 2016; Abbasi et al., 2023), incorporating this dependence, or treating λ_I as a random variable, would not only increase the dimensionality of the parameter space but also affect the definition of the non-interacting thresholds used in this work, thereby complicating the analysis considerably.

In Fig. 1, we illustrate the geometry of the undeformed shell, prior to pressurization, with panels (a) and (b) representing the meridional cross-section and a three-dimensional (3D) view, respectively. A spherical coordinate system (r, θ, ϕ) is used, where $r = R + \sum w_i$ is the radial distance from the origin/center of the sphere, $\theta \in [0, 2\pi]$ is the circumferential angle, and $\phi \in [0, \pi/2]$ is the meridian angle (measured from the pole to the clamped boundary at the equator). The half-angle ϕ_0 defines the cap region within which the defects are seeded, thereby avoiding any interactions with the clamped boundary (Derveni et al., 2023b).

The seeding of the imperfect shell geometry containing a distribution of N non-interacting localized defects was done using a procedure similar to that introduced in Ref. Derveni et al. (2023b), to which we point the reader for additional details. For completeness, a summary of this procedure is outlined next. The angular positions of the center of each defect (θ_i, ϕ_i) are generated uniformly using a random sequential absorption algorithm. Specifically, the locations of each defect are calculated as

$$\left(\theta_i, \phi_i\right) = \left(2\pi q_\theta, \arccos(1 - q_\phi(1 - \cos\phi_0)\right), \tag{19}$$

where $q_\theta, q_\phi \in [0, 1]$ are independent random variables sampled from a uniform distribution. The sampling method in Eq. 19 ensures an equal probability of the placement of defects on a spherical surface. The defect amplitudes $\bar{\delta}_i$ were sampled from a lognormal distribution, defined with prescribed mean $\mu_{\bar{\delta}}$ and standard deviation $\Delta\bar{\delta}$. The angular separation between two defects introduced during the seeding algorithm, i and j, can be computed as $\psi(i, j) = |\arccos(\mathbf{e}_{\mathbf{r}i} \cdot \mathbf{e}_{\mathbf{r}j})|$, where $\mathbf{e}_{\mathbf{r}i}$ is the unit position vector pointing from the origin to the center of the i-th defect. In order to avoid overlaps and interactions between neighboring defects, a minimum angular separation $\psi_{\min}$ was enforced between defect centers. As evidenced by Derveni et al. (2023a), the threshold arclength separation l_p,

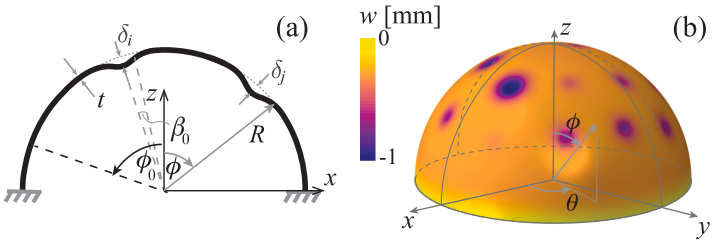

Fig. 1. Geometry of a typical spherical shell with statistically distributed Gaussian dimples, clamped at its free boundary. (a) Meridian cross-section of the shell, defining all the relevant geometric parameters. (b) 3D visualization of a shell in the spherical coordinate system; the color map represents the radial deviation, w, from a perfect sphere.

beyond which defect interactions become negligible is given by $l_p = l_c\left(1 + \frac{\lambda_{Ii}+\lambda_{Ij}}{2\sqrt{2}\pi}\right)$ where l_c denotes the theoretical wavelength of the axisymmetric mode (Hutchinson, 1967),

$$l_c = 2\pi[12(1-\nu^2)]^{-1/4}\sqrt{Rt}. \tag{20}$$

Accordingly, the minimum angular separation, $\psi_{\min}$, between two neighboring defects was set to l_p/R, to ensure no defect-defect interactions.

The finite element simulations assumed an incompressible, hyperelastic neoHookean material model, with a Young's modulus $E = 1.26$ MPa and a Poisson's ratio $\nu = 0.5$; these specific parameters were chosen to be consistent with the previous studies (Derveni et al., 2023a,b) in which comparison and validation against experiments were established. Despite this choice, the FE results presented in the manuscript are expected to be general, as the imperfection sensitivity of thin spherical shells under elastic buckling depends on geometric and load parameters, rather than material properties. In line with prior studies (Derveni et al., 2023a; Jiménez et al., 2017; Lee et al., 2016; Ubamanyu et al., 2025), the buckling analysis was performed using the Static/Riks method, an arclength-based procedure in Abaqus/Standard. This arclength-controlled algorithm solves for both load and displacement simultaneously by advancing along the equilibrium path, making it well-suited for instability problems (Riks, 1979). For each buckling test, a uniform external live pressure, equal to the classical theoretical buckling pressure in Eq. 1, was defined as the nominal load on the outer surface of the shell. We set the initial, minimum, and maximum arc-length increments to 0.01, 10^{-15}, and 0.02, respectively, to ensure numerical stability and robust convergence throughout the simulations (Ubamanyu et al., 2025). For each FE simulation, the knockdown factor, κ, is defined as in Section 2, where the measured onset of buckling is identified as the first peak pressure during loading, obtained from the Riks analysis.

Following the methodology described above, a systematic and large-scale simulation campaign was conducted to investigate how geometry and system size influence imperfection sensitivity in the buckling of spherical shells. Table 1 summarizes all relevant geometric and statistical parameters for each simulation set, namely: radius R, thickness t, half angle of the spherical cap where the defects are placed ϕ_0, minimum angular separation between the center of the defects $\psi_{\min}$, mean $\mu_{\bar{\delta}}$ and standard deviation $\Delta\bar{\delta}$ of the defect amplitude, the average number of defects in a realization $\overline{N}$, and the number of stochastic realizations n_r. We shall refer to a '*stochastic realization*' as a finite element simulation in which a unique, randomly generated distribution of discrete dimple-like defects is applied to an otherwise identical, perfect shell geometry.

Throughout, the theoretical buckling wavelength of the axisymmetric mode l_c was held constant, ensuring a consistent reference length scale across different geometries. The amplitudes of the defects were drawn from a lognormal distribution with a fixed mean value $\mu_{\bar{\delta}} = 0.25$ and standard deviation $\Delta\bar{\delta} = 0.1$. Note that the lognormal distribution satisfies the Von Mises condition (Eq. 8), and therefore the maximum amplitude of a very large number of defects would asymptotically approach a Gumbel distribution. To ensure statistical convergence of the knockdown factor distribution, we generated large ensembles of statistically identical realizations for each case, with the number of realizations n_r ranging between 500 and 2000; see Table 1. Larger sample sizes (up to 2000) were used for cases exhibiting a larger statistical spread in knockdown factors from the mean value. By sampling from the same statistical distribution under consistent geometric constraints, the influence of imperfection randomness on buckling behavior is isolated.

As detailed in Table 1, our simulation campaign consisted of two subsets, (a) and (b), each designed to explore different aspects of how the obtained knockdown factor statistics are affected by geometric and finite-size effects, as follows:

- In subset (a), the effects of varying the shell size are explored by considering hemispherical shells with radii in the range of $R \in [25.4, 100]$ mm, while the shell thickness t is adjusted accordingly to maintain a constant buckling wavelength l_c through Eq. (20). The region over which imperfections were distributed was held fixed at $\phi_0 = 60°$. As R increases, the surface area available for defect placement increases proportionally, allowing more non-interacting defects within the specified region. Because l_c is held constant while R varies, the minimum angular separation between defect centers adjusts according to $\psi_{\min} = l_p/R$, resulting in values spanning $\psi_{\min} \in [6.4°, 25°]$.
- In subset (b), the shell geometry is fixed at $R = 100$ mm and $t = 0.065$ mm (*i.e.*, $R/t = 1550$), while systematically varying the region in the shell where defects can be seeded in the range of $\phi_0 \in [20°, 60°]$. Reducing ϕ_0 limits the area where imperfections may occur, effectively reducing the possible total number of defects.

Table 1
Design parameters for the ensemble of the shells generated for the statistical simulations: radius R and thickness t of the shell, half angle of the spherical cap where the defects are placed ϕ_0, minimum angular separation between the center of the defects $\psi_{\min}$, mean $\mu_{\bar{\delta}}$ and standard deviation $\Delta\bar{\delta}$ of the defect amplitude, the average number of defects in a realization $\overline{N}$, the total number of simulated realizations n_r.

R [mm]	t [mm]	R/t [-]	ϕ_0 [°]	$\psi_{\min}$ [°]	$\mu_{\bar{\delta}}$ [-]	$\Delta\bar{\delta}$ [-]	$\overline{N}$ [-]	n_r [-]
(a) Constant $\phi_0 = 60°$, varying R/t								
25.4	0.254	100	60	25.0	0.25	0.1	14	500
35.0	0.184	190	60	18.1	0.25	0.1	25	500
50.0	0.129	388	60	12.7	0.25	0.1	48	500
75.0	0.086	872	60	8.5	0.25	0.1	102	500
100.0	0.065	1550	60	6.4	0.25	0.1	174	500
(b) Constant $R/t = 1550$, varying ϕ_0								
100.0	0.065	1550	60	6.4	0.25	0.1	174	500
100.0	0.065	1550	50	6.4	0.25	0.1	127	500
100.0	0.065	1550	40	6.4	0.25	0.1	86	500
100.0	0.065	1550	30	6.4	0.25	0.1	52	2000
100.0	0.065	1550	20	6.4	0.25	0.1	25	2000

Both subsets (a) and (b) can be used to investigate the effect of the number of defects on the statistics of the knockdown factor. The main difference between these two parts lies in how they produce varying numbers of defects. In subset (a), the total area of the defect zone is varied by changing the shell radius. Since the minimum distance between two defects is dictated by the length scale $\sqrt{Rt}$, it can be concluded that the number of defects in subset (a) is governed by the shell dimension. By contrast, in subset (b), the total area of the defect zone and the number of defects are governed solely by the half angle ϕ_0.

It is worthwhile to mention that, if R/t is chosen as a means of changing the number of defects, its variation could affect the relationship between the knockdown factor and the normalized defect amplitude, i.e., the $\kappa(\delta)$ curve (Jiménez et al., 2017). In turn, a different $\kappa(\delta)$ curve would consequently change the probability distribution of knockdown factor corresponding to a single defect (function $F_{\kappa_1}(\kappa)$ in Eq. 4). However, as we will evidence in the next section, for subset (a) of the current simulations, where the R/t ratio is considerably large, the dependence of the $\kappa(\delta)$ relationship on R/t is negligible.

4. Validation of the analytical model

In this section, we validate the individual components of the analytical model introduced in Section 2, which include 1) the dependence of the knockdown factor on the defect amplitude (Eq. 3); 2) the randomness in the number of non-interacting defects and the justification for using the average defect number in the weakest-link model (Eq. 16); and 3) the weakest-link framework for extrapolating the CDFs of the knockdown factor of shells with different numbers of defects. The analytically predicted CDFs of the knockdown factor are then compared with the results of SFE simulations.

4.1. Relationship between knockdown factor and defect amplitude for shells with a single defect

The relationship between the knockdown factor and defect amplitude (i.e., Eq. 3) is the key input to the proposed analytical model. To quantify this relationship for different dimensionless radii considered in subset (a) of the simulations, we performed an FE analysis of buckling of shells with a single Gaussian dimple defect located at the pole, yielding the $\kappa(\bar{\delta})$ curves presented in Fig. 2a. For the considered R/t range, the $\kappa(\bar{\delta})$ relationship shows only mild R/t dependence, consistently with (Jiménez et al., 2017), where it was found that at large R/t it is primarily governed by the defect-width parameter λ_I. Therefore, in this study, the $\kappa(\bar{\delta})$ curves were averaged over all R/t and the average response was fitted using Eq. 3 (see Fig. 2b), yielding the fitting parameters $\kappa_0 = 0.45$, $a = 0.51 \pm 0.01$, and $b = 3.88 \pm 0.08$. The reported uncertainties represent the 95 % confidence intervals for the parameter estimates. These values were used as an input to Eq. 3 for predicting the probability distribution of knockdown factors of shells considered in subset (a) of the simulations.

For subset (b) of the simulations, all cases have the same dimensionless radii ($R/t = 1550$). Therefore, Eq. 3 was used directly to fit the simulated $\kappa(\bar{\delta})$ curve for $R/t = 1550$ (with $\kappa_0 = 0.448$, $a = 0.54 \pm 0.01$, and $b = 3.73 \pm 0.10$) in the subsequent calculation of the knockdown factor distributions. It is important to note that the chosen probability distribution of defect amplitude $\bar{\delta}$ and defect width lead to relatively high knockdown factors.

4.2. Randomness of the number of non-interacting defects

The weakest-link statistical model requires knowledge of the number of non-interacting defects for a given shell, which physically represents the number of potential locations where localized buckling could occur. In the SFE simulations, the defects were placed sequentially on the shell with the minimum distance constraint by using a random absorption algorithm (cf. Section 3). Depending on the locations of the first few defects, the number of generated defects may differ between individual realizations. It is expected

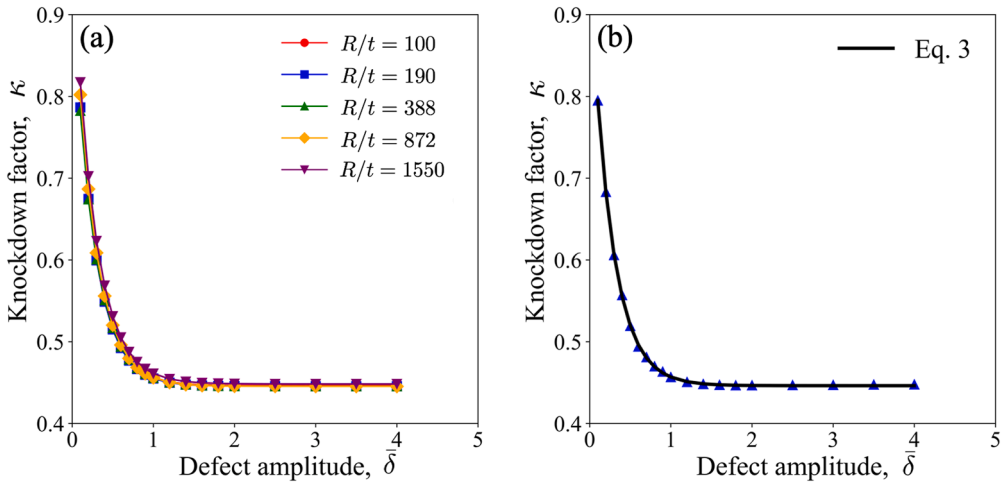

Fig. 2. (a) Simulated $\kappa(\bar{\delta})$ relationship for shells of different geometries. (b) The average response fitted by Eq. 3 is used in the analytical model.

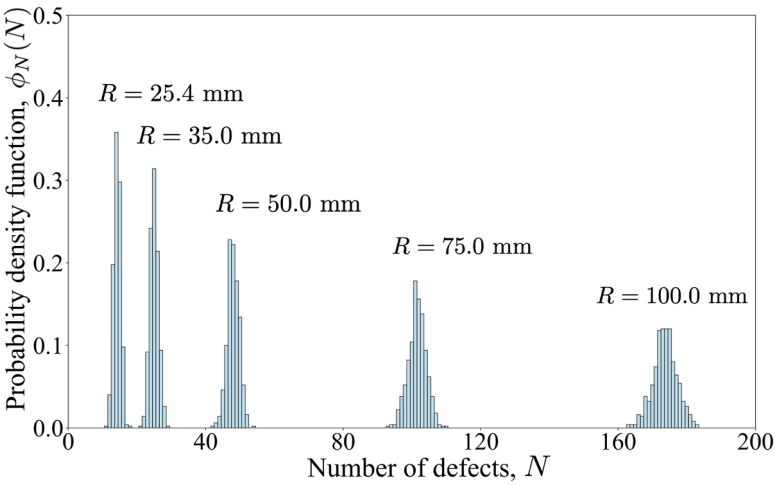

Fig. 3. Histograms of defect number N for shells of five sizes $R = \{25.4,\ 35.0,\ 50.0,\ 75.0$ and $100.0\}$ mm showing that both the mean and standard deviation of the defect number increase with the shell size, but the CoV of defect number decreases with the shell size.

that the shell size influences the randomness of the defect number. As a demonstration, Fig. 3 shows the distributions of defect numbers for different cases of subset (a) of the simulations. It is seen that the CoV of the defect number decreases as the shell radius increases: 7.3 % for $R = 25.4$ mm, 5.1 % for $R = 35.0$ mm, 3.6 % for $R = 50.0$ mm, 2.6 % for $R = 75.0$ mm, and 2.0 % for $R = 100.0$ mm. This simulated trend can be explained by the fact that the effect on the placements of the first few defects on the total number of defects diminishes as the shell size increases. When the shell becomes sufficiently large, the defect number approaches a deterministic quantity.

To check the applicability of Eq. 16 to the present study, the CDFs of knockdown factor of shells with the smallest defect zone are compared (first case of subset (a) of the simulation: $R = 25.4$, $t = 0.254$ mm) by using Eq. 15 and Eq. 16. As seen in Fig. 4, the knockdown factor distributions computed by Eqs. 15 and 16 are indistinguishable, which validates the use of Eq. 16. Eqs. 15 and 16 agree because, with a relatively small CoV of defect number (approximately 7.3 %), we may approximate $\mathbb{E}_N\left\{\ln\left[1 - F_{\kappa_N}(\kappa)\right]\right\}$ by $\ln\left\{1 - \mathbb{E}_N[F_{\kappa_N}(\kappa)]\right\}$ ($\mathbb{E}_N(\cdot)$ denotes the mathematical expectation with respect to defect number N). Since all other simulation cases have a larger number of defects and a lower CoV of defect number, Eq. 16 is sufficient for the calculation of knockdown factor distributions of all cases considered in the present SFE simulations.

4.3. Validation of weakest-link model

The salient feature of the weakest-link model (Eq. 16) is that it directly relates the CDFs of the knockdown factor of shells of the same size but containing different numbers of defects. Now, consider two shells of the same size but containing $\bar{N}_1$ and $\bar{N}_2$ numbers

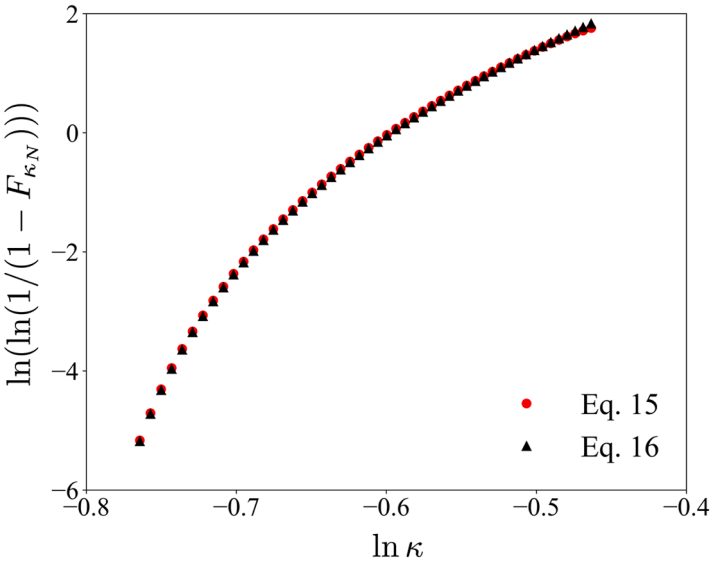

Fig. 4. Comparison of the predicted CDFs of the knockdown factor $F_{\kappa_N}(\kappa)$ using Eqs. 15 and 16.

of defects. By applying Eq. 16 to both shells and eliminating the CDF $F_{\bar{\delta}}[g^{-1}(\kappa)]$ of the defect amplitude, we obtain

$$F_{\kappa}(\kappa, \bar{N}_2) = 1 - \left[1 - F_{\kappa}(\kappa, \bar{N}_1)\right]^{\bar{N}_2/\bar{N}_1}. \tag{21}$$

Next, we use the results from the subset (b) of the simulations to check the validity of Eq. 21. Shells with $\phi_0 = 20°$ are chosen as the reference case, and Eq. 21 is used to predict the probability distributions of knockdown factors of shells with other ϕ_0 values. To determine the CDF of the knockdown factor of the reference case, we first calibrate the $\kappa(\bar{\delta})$ curve so that Eq. 6 provides an optimum fit of the simulated CDF of the knockdown factor. In the calibration, the threshold value κ_0 is fixed to be 0.448 based on the simulated $\kappa(\bar{\delta})$ curve (Fig. 2), while the parameters a and b are used as free fitting parameters for the calibration, and the average defect number $\bar{N} = 25$ is used for Eq. 6. As seen in Fig. 5a, Eq. 6 can provide an optimal fit to the simulation results. This calibration yields $a^* = 0.575$ and $b^* = 3.975$, which is very close to the result of direct fitting of the simulated $\kappa(\bar{\delta})$ curve shown in Fig. 2b ($a = 0.536$, and $b = 3.734$).

With the calibrated $\kappa(\bar{\delta})$ curve, Eq. 6 provides an analytical distribution function for shells with $\phi_0 = 20°$. Eq. 21 is then used to predict the CDFs of the knockdown factor of shells with $\phi_0 = 40°, 50°$, and $60°$ (the corresponding average numbers of defects are 86, 127, and 174). Fig. 5b-d compare the prediction of Eq. 21 with the simulation results. It is noted that the simulated CDF is not perfectly smooth for two reasons: 1) the number of realizations in the SFE simulations is rather limited, and 2) we directly sample the random defect amplitude, which, owing to the nonlinear relationship between the defect amplitude and knockdown factor, leads to a set of uneven spaced random knockdown values. Nevertheless, the analytical prediction agrees very well with the simulation results. These findings provide direct evidence of the applicability of the weakest-link model for the statistics of knockdown factor, consistently with the recent study by Derveni *et al.*, which showed that the buckling pressure of a hemispherical shell containing multiple non-interacting defects is governed solely by the behavior of the most severe defect (Derveni et al., 2025).

4.4. Direct prediction of knockdown factor distribution from the $\kappa(\bar{\delta})$ relationship

The proposed analytical model is now used to predict the statistics of the knockdown factor directly from the $\kappa(\bar{\delta})$ relationship. As mentioned previously, for the subset (a) of the simulations, which comprises cases of different R/t ratios, the differences among $\kappa(\bar{\delta})$ curves for different R/t ratios are minor. Therefore, the average behavior of the $\kappa(\bar{\delta})$ curve (Fig. 2b) is used in the analytical model. By contrast, all cases of the subset (b) have the same R/t ratio, and the $\kappa(\bar{\delta})$ curve corresponding to that particular R/t ratio is used in the subsequent calculation.

Fig. 6 and Fig. 7 present the comparison between the analytically predicted and numerically simulated CDFs of knockdown factor on a two-parameter Weibull probability plot for the simulation subsets (a) and (b), respectively. For all cases, we find that the simulated knockdown factor distributions approach a vertical asymptote at small buckling probabilities, suggesting a minimum threshold value κ_0 under which the chance of a shell with dimple defects of random amplitudes is zero. This is consistent with the simulated $\kappa(\bar{\delta})$ relationship (Fig. 2a), which exhibits a knockdown threshold at large values of the defect amplitude.

In Figs. 6 and 7, we also juxtapose the analytical model (Eq. 16 as solid black lines) with the data obtained from SFE simulations (blue dots), revealing good agreement between the two, albeit with some minor differences. However, it should be noted that the Weibull probability plot uses the logarithmic scale of the knockdown factor. The actual difference between the analytical and

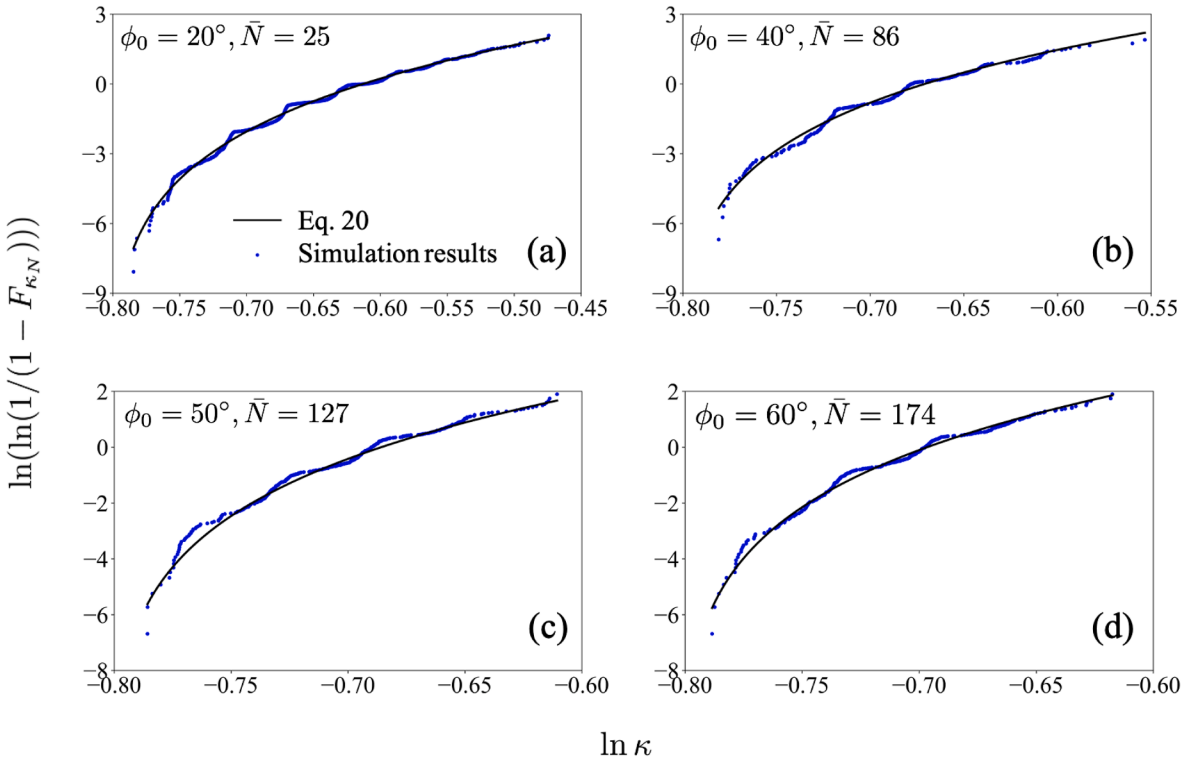

Fig. 5. (a) Optimum fitting of the simulated CDF of knockdown factor for $\phi_0 = 20°$, and (b)-(d) Comparison of the simulated CDFs of knockdown factor and those extrapolated from the reference case $\phi_0 = 20°$.

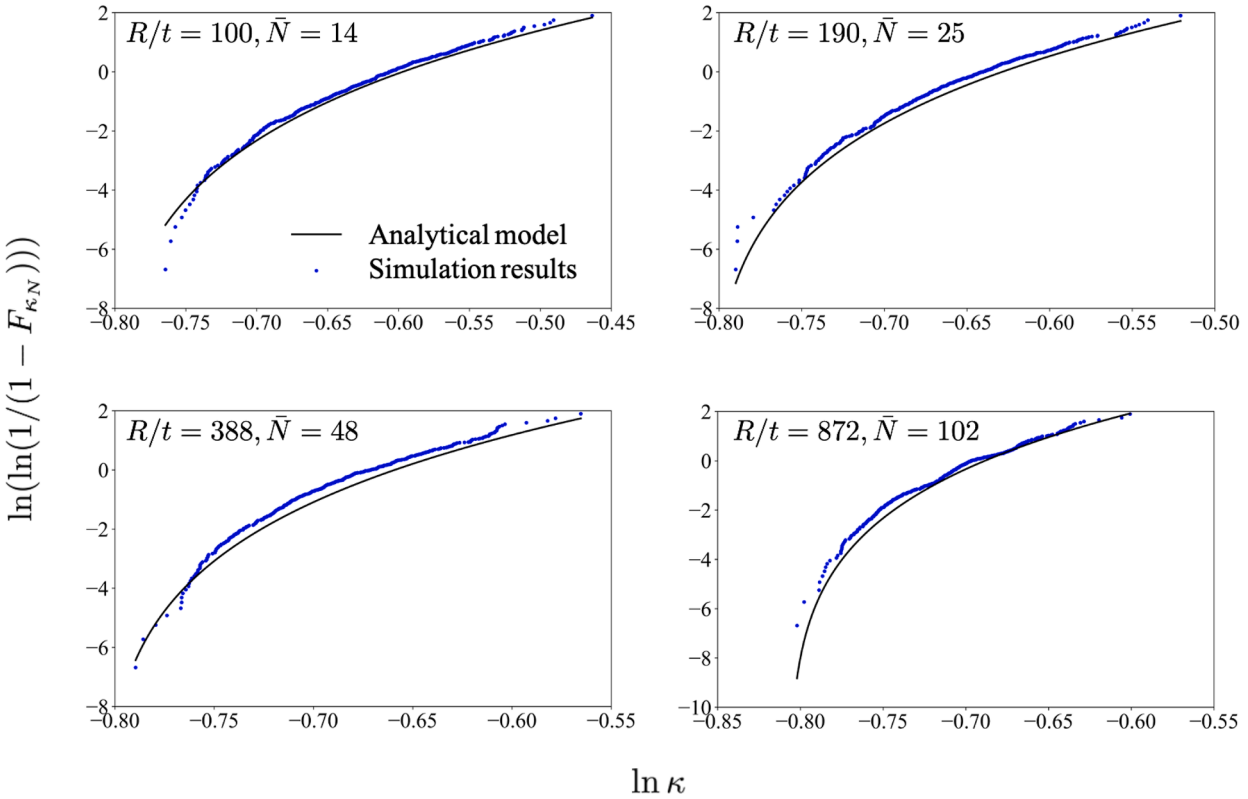

Fig. 6. Comparison of the analytical model and SFE simulation data for subset (a) presented on two-parameter Weibull probability plot.

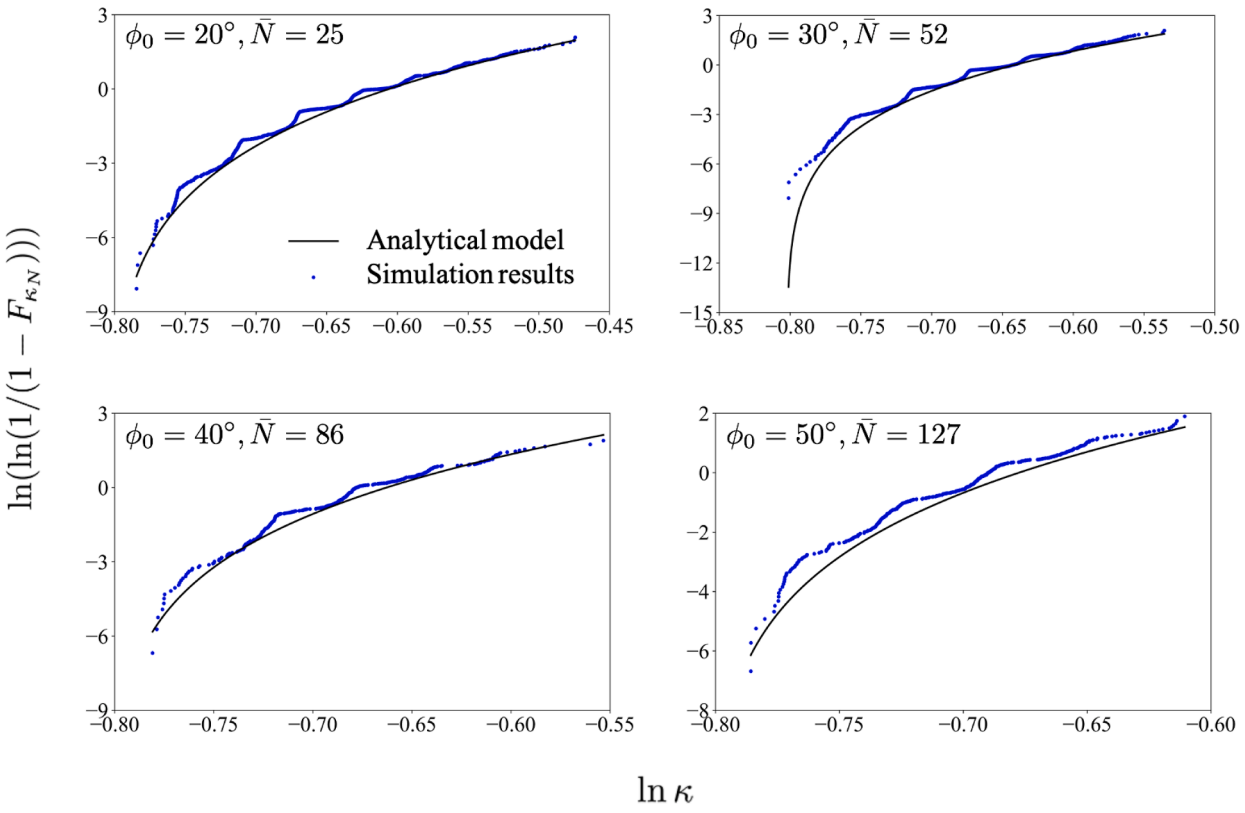

Fig. 7. Comparison of the analytical model and SFE simulation data for subset (b) presented on two-parameter Weibull probability plot.

Table 2
Norm of relative error between the analytical model and stochastic SFE simulation results.

	R [mm]	R/t [-]	ϕ_0 [°]	Norm of relative error [%]
Subset (a)	25.4	100	60	0.895
	35.0	190	60	1.157
	50.0	388	60	1.177
	75.0	872	60	0.577
	100.0	1550	60	0.869
Subset (b)	100.0	1550	60	0.869
	100.0	1550	50	1.064
	100.0	1550	40	0.873
	100.0	1550	30	0.834
	100.0	1550	20	0.836

simulation results can be quantified through the norm of relative error

$$\varepsilon = \sqrt{\frac{\sum_{i=1}^{n_r} |\kappa_{\text{model},i} - \kappa_{\text{sim},i}|^2}{\sum_{i=1}^{n_r} (\kappa_{\text{sim},i})^2}} \times 100\,\%, \tag{22}$$

where n_r = total number of realization for a given shell geometry, $\kappa_{\text{sim},i}$ = simulated knockdown factor for i-th realization, which corresponds to failure probability P_i, and $\kappa_{\text{model},i} = F_{\kappa}^{-1}(P_i)$ = the analytically predicted knockdown factor corresponding to P_i. The results for this error norm are represented in Table 2. In all cases, we find that the norm of relative error is below 1.2 %, providing a validation of the proposed analytical model for predicting the CDF of the knockdown factor directly from the $\kappa(\bar{\delta})$ relationship.

In Section 2, we demonstrated that the CDF of knockdown factor approaches the three-parameter Weibull distribution as the defect number becomes very large. In Fig. 8, we present the predicted and simulated CDFs of knockdown factor on a three-parameter Weibull probability plot for the case of $R/t = 1550$ and $\phi_0 = 60°$, which corresponds to the shell containing the largest number of dimple defects ($\bar{N} = 174$) in the present study. The threshold κ_0 in the three-parameter Weibull probability plot is fixed at the threshold value of the $\kappa(\bar{\delta})$ curve shown in Fig. 2b. From the data in Fig. 8, on the three-parameter Weibull plot, we conclude that

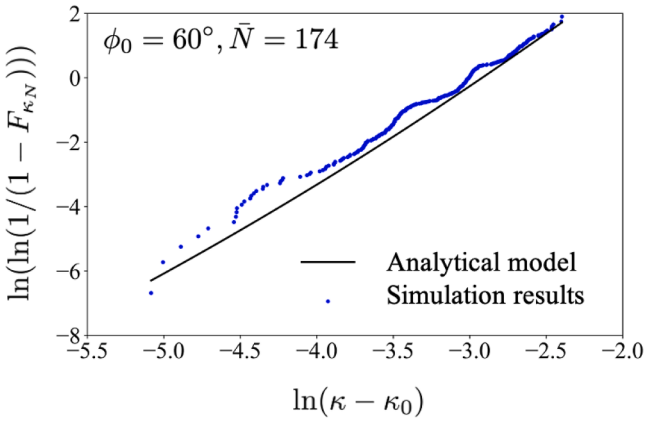

Fig. 8. Comparison of the analytical model and SFE simulation data for $R/t = 1550$ and $\phi_0 = 60°$ with an average defect number $\bar{N} = 174$ presented on three-parameter Weibull probability plot.

the knockdown factor distribution does not follow a straight line, indicating that the number of defects considered in the present simulation is not sufficiently large to approach asymptotically the three-parameter Weibull distribution.

As indicated by Eqs. 9 and 10, the CDF of the knockdown factor would approach the three-parameter Weibull distribution when the CDF of the maximum defect amplitude can be reasonably described by the Gumbel distribution. Due to the heavy right tail of the lognormal distribution, the convergence of the maximum of lognormally distributed random variables to the Gumbel distribution is rather slow, on the order of $O(1/\ln \bar{N})$ (Hall, 1979). Therefore, we estimate that the number of defects required for the maximum defect amplitude to be reasonably approximated (with an error of 10 % or less) by the Gumbel distribution would be at least on the order of tens of thousands, which is significantly larger than the largest value considered here: $\bar{N} = 174$.

5. Size effect on the statistics of knockdown factor

We now use the results of the SFE simulations to investigate the statistical size effect mentioned in Section 2 (Eq. 18). In the present simulations, the statistical size effect can be obtained by either changing the overall shell size (subset (a) of the simulations) or changing the size of the imperfection cap (subset (b) of the simulations).

Fig. 9 shows the simulated size effects on the mean value, $\bar{\kappa}$, and CoV, ω_κ, of the knockdown factor. In both cases, we find that $\bar{\kappa}$ and ω_κ decrease with an increasing number of defects, $\bar{N}$. The size effect on the mean knockdown factor can be attributed to the fact that, as the number of defects increases, it is more likely that a defect with a larger amplitude is sampled (or equivalently, a smaller knockdown factor is sampled). Therefore, the mean knockdown factor decreases as the defect number increases. The size effect on the CoV of the knockdown factor can be understood by noting that the CDF of the overall knockdown factor of the shell is determined by the left portion of the CDF of the knockdown factor of a single defect, and that portion becomes smaller as the number of defects increases. Since the knockdown factor of a single defect exhibits a threshold, it is evident that the randomness of the knockdown factor of a single defect decreases as the probability decreases. Consequently, the CoV of the knockdown factor of the shell decreases with an increasing defect number.

In the limiting case of an infinite number of defects, the CDF of the knockdown factor of the shell is governed by the extreme left tail of the CDF of the knockdown factor of a single defect, which exhibits no randomness. The knockdown factor corresponds to its threshold value κ_0. Therefore, we conclude that, as the defect number increases to infinity, the mean knockdown factor would approach the knockdown threshold, κ_0, and the CoV of the knockdown factor would approach zero. In other words, the knockdown factor of the shell exhibits no randomness even though the individual defect has a random amplitude.

Based on the weakest-link model (Eq. 16), the mean value and CoV of the knockdown factor can be calculated by

$$\bar{\kappa}(\bar{N}) = \int_0^\infty [1 - F_\kappa(\kappa)]\mathrm{d}\kappa = \int_0^\infty \left\{F_{\tilde{\delta}}[g^{-1}(\kappa)]\right\}^{\bar{N}} \mathrm{d}\kappa \tag{23}$$

$$\omega_\kappa(\bar{N}) = \frac{1}{\bar{\kappa}(N)} \left\{ \int_0^\infty \kappa^2 \bar{N} \left\{F_{\tilde{\delta}}[g^{-1}(\kappa)]\right\}^{\bar{N}-1} \frac{\mathrm{d}F_{\tilde{\delta}}[g^{-1}(\kappa)]}{\mathrm{d}\kappa} \mathrm{d}\kappa - [\bar{\kappa}(N)]^2 \right\}^{1/2} \tag{24}$$

Since the behavior of a single defect (i.e., the $\kappa(\tilde{\delta})$ curve) for both subsets (a) and (b), of the simulations are very close to each other, we plot the computed size effects on the mean and CoV of knockdown factor by combining the results of subsets (a) and (b) together with the prediction of the analytical model by using the averaged $\kappa(\tilde{\delta})$ curve obtained from subset (a) of the simulations, as shown in Fig. 9. It is seen that the analytical model (Eqs. 23 and 24) matches the simulation results very well.

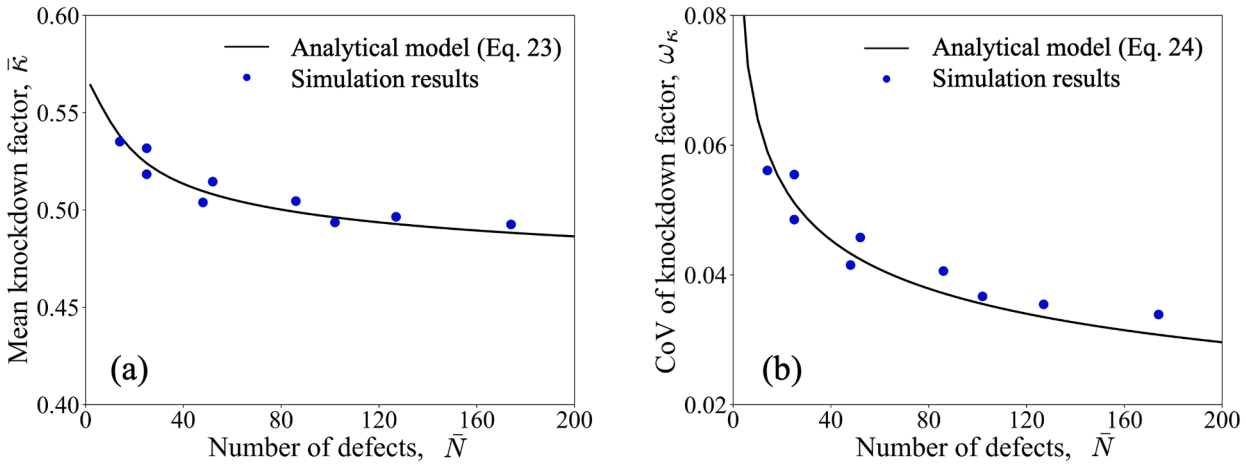

Fig. 9. Simulated size effects on (a) the mean value and (b) CoV of the knockdown factor and their comparisons with analytical model (Eqs. 23 and 24).

Based on the aforementioned large-size asymptotic behaviors of $\bar{\kappa}(\bar{N})$ and $\omega_\kappa(\bar{N})$, the following approximate equations are proposed for the size effects on the mean and CoV of the knockdown factor in lieu of Eqs. 23 and 24:

$$\bar{\kappa}(\bar{N}) = \kappa_0\left(1 + \frac{N_0}{\bar{N}}\right)^{1/r} \tag{25}$$

$$\omega_\kappa(\bar{N}) = \omega_0 \exp\left[-(\bar{N}/N_1)^q\right], \tag{26}$$

where N_0, N_1, r, q, and ω_0 are constants for a given shell geometry. Clearly κ_0 must equal the threshold value of the knockdown factor indicated by the $\kappa(\bar{\delta})$ curve. At the small size limit (small values of $\bar{N}$), Eqs. 25 and 26 are approximated by $\bar{\kappa}(\bar{N}) \approx \kappa_0(N_0/\bar{N})^{1/r}$ and $\omega_\kappa(\bar{N}) \approx \omega_0[1 - (\bar{N}/N_1)^q]$, respectively. Therefore, the constants $N_0, r, \omega_\kappa, N_1$, and q can be determined by optimum fits of the behavior of Eqs. 23 and 24 for small values of $\bar{N}$.

The degree of the statistical size effect is primarily governed by the CoV of the knockdown factor ω_{κ_1} of shells containing only one defect. If ω_{κ_1} is small, the random values sampled for each individual defect do not vary significantly from each other. Therefore, the smallest knockdown factor of the defects would vary mildly with the number of defects, suggesting a weak statistical size effect. In the limiting case, when ω_{κ_1} is zero, the statistical size effect vanishes since the mean knockdown factor of the shell containing any number of defects is equal to the knockdown factor of the shell containing one defect. Based on Eq. 4, the CoV of ω_{κ_1} is governed by the CDF of the dimple amplitude and the $\kappa(\bar{\delta})$ relationship. It has been shown that the $\kappa(\bar{\delta})$ relationship depends on the R/t ratio when R/t is small (Jiménez et al., 2017). Therefore, strictly speaking, we should treat the model parameters N_0, N_1, r, q, ω_0, and κ_0 as functions of R/t. Nevertheless, Fig. 2a shows that, for the range of R/t considered in the present study, the $\kappa(\bar{\delta})$ relationships of all the simulation cases are nearly identical, suggesting that, here, we can consider all the model parameters in Eqs. 25 and 26 are independent of R/t.

In Section 2, we discussed that the maximum number of non-interacting defects in a given hemispherical shell scales linearly with R/t (Eq. 17). To validate it, we plot the calculated average maximum numbers of defects for shells with different R/t ratios based on the subset (a) of the simulations together with its optimum fit by a linear relationship $\bar{N} = 0.11R/t$ (Fig. 10). By substituting this linear relationship into Eqs. 25 and 26, we express the statistical size effects on the mean and CoV of knockdown factors in terms of R/t:

$$\bar{\kappa} = \kappa_0\left\{1 + \frac{\eta_1}{R/t}\right\}^{1/r} \tag{27}$$

$$\omega_\kappa = \omega_0 \exp\left[-\eta_2(R/t)^q\right] \tag{28}$$

where η_1, η_2 = constants. It is noted that Eq. 27 can be recast in the form of Eq. 18 with $\Psi(R/t) = [1 + \eta_1/(R/t)]^{1/r}(\kappa_0/\kappa_1)$.

Fig. 11 shows that Eqs. 27 and 28 provide optimum fitting of the size effects on the mean and CoV of knockdown factor predicted by the analytical model (Eqs. 23 and 24) over a wide range of defect numbers. Based on Fig. 2b, $\kappa_0 = 0.446$ for the present simulation cases. The optimum fitting yields the values of rest parameters: $\eta_1 = 31612, r = 33, \omega_0 = 0.14, \eta_2 = 0.37$, and $q = 0.19$. The large value of r indicates that the size effect on the mean knockdown factor is weak. To explain this, we note that the defect amplitude exhibits a considerable degree of randomness (CoV of $\bar{\delta} = 40\,\%$). However, due to the nonlinear $\kappa(\bar{\delta})$ relationship, the corresponding randomness of the knockdown factor is moderately low (the CoV of the knockdown factor of shells containing a single defect $F_{\kappa_1}(\kappa)$ is approximately 10.4 %), which leads to a weaker statistical size effect on the mean knockdown factor.

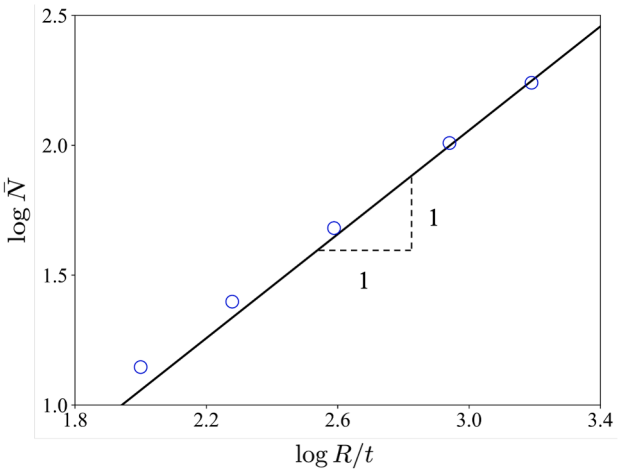

Fig. 10. Simulated relationship between the average maximum number of non-interacting defects $\bar{N}$ and dimensionless radius R/t and its optimum fit by a linear function.

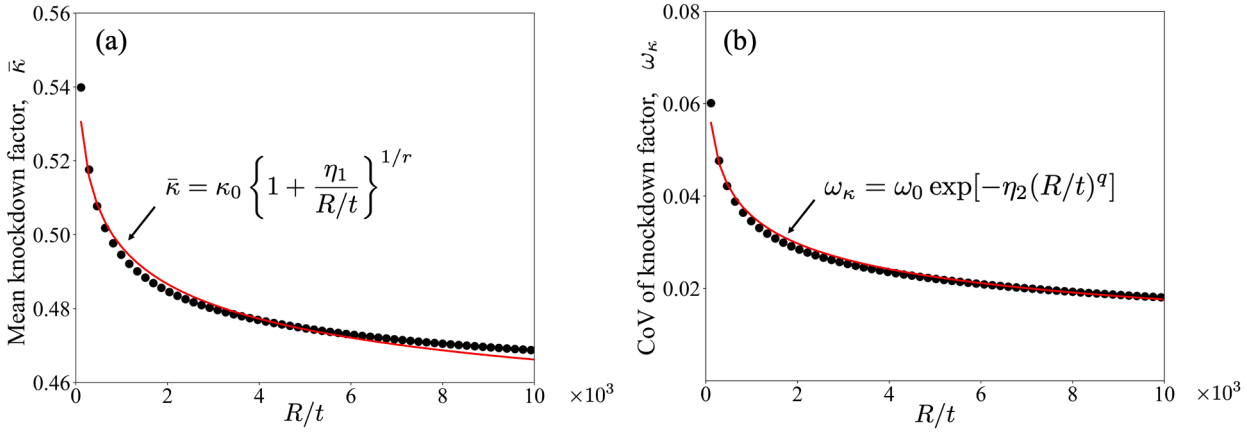

Fig. 11. Statistical size effects on the knockdown factor predicted by the analytical model (23 and 24) and their optimum fits by Eqs. 27 and 28: (a) mean knockdown factor and (b) CoV of the knockdown factor.

6. Conclusions

This study showed that the statistics of the knockdown factor of hemispherical shells containing a distribution of non-interacting localized defects can be well described by a finite weakest-link model. The success of the model is attributed to the fact that the knockdown factor is dictated only by the most severe defect. Using the knowledge of the buckling behavior of shells containing a single defect, the probability distribution of the knockdown factor of those containing multiple defects is related directly to the statistics of the defect amplitude. If the probability distribution function of the defect amplitude satisfies the Von Mises condition for the Gumbel domain of attraction, the knockdown factor asymptotically approaches a three-parameter Weibull distribution as the number of defects becomes large. The convergence rate to this asymptotic distribution is rather slow for the case of lognormally distributed defect amplitudes, but would increase if exponentially distributed defect amplitudes are considered.

The developed analytical model readily predicts the statistical size effect, which describes the effect of defect number on the statistics of the knockdown factor. By considering the conservative case of the shell fully containing non-interacting defects, it was shown that the maximum number of defects is governed by the dimensionless radius R/t. Consequently, R/t governs the statistical size effects on the mean and CoV of the knockdown factor, information which is hidden within available test data. The analytical model was validated by a large set of SFE simulations of hemispherical shells with different geometrical dimensions and of different sizes of the imperfection zone. The simulations yielded the probability distribution of the knockdown factor, which was shown to agree very well with the analytical model.

In this study, we computed the CDF of the knockdown factor, $F_\kappa(\kappa)$, by considering non-interacting defects with random amplitudes and a constant defect-width parameter, λ_I. In a more general setting, however, the amplitude, width, and spacing of defects may be treated as spatial random variables, in which case defect interactions naturally arise. An efficient way to represent such

imperfections is through a random field representation, as proposed in (Baizhikova et al., 2024). Importantly, it has been demonstrated that in that case the weakest-link model remains valid for capturing the statistics of the knockdown factor (Baizhikova et al., 2024). Taken together, the present results and those of Baizhikova et al. (2024) suggest that the weakest-link model can serve as a general framework for describing the statistics of buckling pressure in spherical and hemispherical shells with diverse types of random geometric imperfections. In a broader context, the weakest-link model is also expected to be applicable to other imperfection-sensitive thin shells, such as axially compressed cylindrical shells, which exhibit localization-induced failures.

Finally, it is worth noting that the proposed weakest-link model provides a natural framework for reliability-based design of hemispherical shells. When combined with the statistics of applied load, the model can generate families of curves relating the allowable applied pressure to the dimensionless radius R/t for different target failure probabilities. This framework offers a rigorous basis for reliability-based design, in contrast to the more commonly used empirical approaches, where the allowable pressure is simply determined from the lower bound of the test dataset (e.g., Weingarten et al. (1968))

CRediT authorship contribution statement

Zheren Baizhikova: Writing – review & editing, Writing – original draft, Investigation, Formal analysis; **Uba K. Ubamanyu:** Writing – review & editing, Writing – original draft, Investigation, Formal analysis; **Fani Derveni:** Writing – review & editing, Investigation, Formal analysis; **Roberto Ballarini:** Writing – review & editing, Supervision, Conceptualization; **Pedro M. Reis:** Writing – review & editing, Supervision, Methodology; **Jia-Liang Le:** Writing – review & editing, Supervision, Project administration, Methodology, Investigation, Formal analysis, Conceptualization.

Data availability

Data will be made available on request.

Declaration of competing interest

The authors declare that they have no known competing financial interests or personal relationships that could have appeared to influence the work reported in this paper.

Acknowledgments

R. Ballarini acknowledges support from the Thomas and Laura Hsu Professorship.

References

Abbasi, A., Derveni, F., Reis, P.M., 2023. Comparing the buckling strength of spherical shells with dimpled *versus* bumpy defects. J. Appl. Mech. ASME 90 (6), 061008. https://doi.org/10.1115/1.4056801

Amazigo, J.C., 1969. Buckling under axial compression of long cylindrical shells with random axisymmetric imperfections. Quar. Appl. Math. 26 (4), 537–566.

Ang, A.H.-S., Tang, W.H., 1984. Probability Concepts in Engineering Planning and Design. Vol II. Decision, Risk and Reliability. John Wiley & Sons, New York.

Audoly, B., Hutchinson, J.W., 2020. Localization in spherical shell buckling. J. Mech. Phys. Solids 136, 103720.

Baizhikova, Z., Ballarini, R., Le, J.L., 2024. Uncovering the dual role of dimensionless radius in buckling of spherical shells with random geometric imperfection. Proc. Nat'l Acad. Sci. USA 121 (16), e2322415121.

Bažant, Z.P., Cedolin, L., 1991. Stability of Structures: Elastic, Inelastic, Fracture and Damage Theories. Oxford University Press, New York.

Bažant, Z.P., Le, J.L., 2017. Probabilistic Mechanics of Quasibrittle Structures: Strength, Lifetime, and Size Effect. Cambridge University Press, Cambridge, U.K.

Bolotin, V.V., 1962. Statistical Methods in the Nonlinear Theory of Elastic Shells. Technical Report TT F-85. NASA.

Carlson, R.L., Sendelbeck, R.L., Hoff, N.J., 1967. Experimental studies of the buckling of complete spherical shells. Exp. Mech. 7 (7), 281–288.

Daniels, H.E., 1945. The statistical theory of the strength of bundles and threads. Proc. R. Soc. London A. 183, 405–435.

Derveni, F., Abbasi, A., Reis, M.P., 2023a. Defect-defect interactions in the buckling of imperfect spherical shells. J. Appl. Mech. ASME .

Derveni, F., Choquart, F., Abbasi, A., Yan, D., Reis, P., 2025. The most severe imperfection governs the buckling strength of pressurized multi-defect hemispherical shells. Mech. Mater. 204, 105295.

Derveni, F., Gueissaz, W., Yan, D., Reis, P.M., 2023b. Probabilistic buckling of imperfect hemispherical shells containing a distribution of defects. Phil. Trans. R. Soc. A 381, 20220298.

Elishakoff, I., 2000. Uncertain buckling: its past, present and future. Int. J. Solids Struct. 37, 6869–6889.

Elishakoff, I., Arbocz, J., 1985. Reliability of axially compressed cylinderical shells with general nonsymmetric imperfections. J. Appl. Mech., ASME 52 (3), 122–128.

Elishakoff, I., Cai, G.Q., 1994. Nonlinear buckling of a column with initial imperfection via stochastic and non-stochastic convex models. Int. J. Non-Linear Mech. 29, 71–82.

Falk, M., Marohn, F., 1993. Von mises conditions revisited. The Ann. Prob. 21 (3), 1310–1328.

Fraser, W.B., Budiansky, B., 1969. The buckling of a column with random initial deflections. J. Appl. Mech. ASME 36, 232–240.

Haldar, A., Mahadevan, S., 2000. Probability, Reliability, and Statistical Methods in Engineering Design. Wiley, New York.

Hall, P., 1979. On the rate of convergence of normal extremes. J. Appl. Prob. 16, 433–439.

Harlow, D.G., Phoenix, S.L., 1978. The chain-of-bundles probability model for the strength of fibrous materials i: analysis and conjectures. J. Comp. Mater. 12, 195–214.

Homewood, R.H., Brine, A.C., Johnson Jr, A.E., 1961. Experimental investigation of the buckling instability of monocoque shells. Exp. Mech. 1 (3), 88–96.

Hutchinson, J.W., 1967. Imperfection sensitivity of externally pressurized spherical shells. J. Appl. Mech. ASME 34, 49–55.

Hutchinson, J.W., 2016. Buckling of spherical shells revisited. Proceedings of the Royal Society A: Mathematical, Physical and Engineering Sciences 472 (2195), 20160577. https://doi.org/10.1098/rspa.2016.0577

Hutchinson, J.W., Thompson, J.M.T., 2018. Imperfections and energy barriers in shell buckling. Int. J. Solids Struct. 148, 157–168.

Jiménez, F.L., Marthelot, J., Lee, A., Hutchinson, J.W., Reis, P.M., 2017. Knockdown factor for the buckling of spherical shells containing large-amplitude geometric defects. J. Appl. Mech. ASME 84, 034501.

Kaplan, A., Fung, Y.C., 1954. A nonlinear theory of bending and buckling of thin elastic shallow spherical shells. Technical Note 3212. National Advisory Committe for Aeronautics.
Koga, T., Hoff, N.J., 1969. The axisymmetric buckling of initially imperfect complete spherical shells. Int. J. Solids Struct. 5 (7), 679–697. https://doi.org/10.1016/0020-7683(69)90088-2
Le, J.L., 2020. Level excursion analysis of probabilistic quasibrittle fracture. Sci. China: Tech. Sci. 63, 1141–1153.
Le, J.L., 2024. Statistical scaling in localization-induced failures. Appl. Mech. Rev., ASME 76, 060801.
Lee, A., López, J.M., Marthelot, J., Hutchinson, J.W., Reis, P.M., 2016. The geometric role of precisely engineered imperfections on the critical buckling load of spherical elastic shells. J. Appl. Mech., ASME 83 (11), 111005.
von Mises, R., 1936. La distribution de la plus grande de n valeurs. Rev., Math, Union Interbalcanique 1, 141–160.
Riks, E., 1979. An incremental approach to the solution of snapping and buckling problems. Int. J. Solids Struct. 15 (7), 529–551. https://doi.org/10.1016/0020-7683(79)90081-7
Tsien, H.S., 1942. A theory for the buckling of thin shells. J. Aero. Sci. 9 (10), 373–384.
Ubamanyu, U.K., Baizhikova, Z., Le, J.-L., Ballarini, R., Reis, P.M., 2025. A numerical study on the buckling of near-perfect spherical shells. J. Appl. Mech., ASME 92 (5), 051003.
Vanmarcke, E., 2010. Random Fields Analysis and Synthesis. World Scientific Publishers, Singapore.
Von Kármán, T., Tsien, H.S., 1939. The buckling of spherical shells by external pressure. J. Aero. Sci. 7 (2), 43–50.
Wang, H., Guilleminot, J., Schafer, B.W., Tootkaboni, M., 2022. Stochastic analysis of geometrically imperfect thin cylindrical shells using topology-aware uncertainty models. Comput. Methods Appl. Mech. Engrg. 393, 114780.
Weibull, W., 1939. The phenomenon of rupture in solids. Proc. Royal Sweden Inst. Engrg. Res. 153, 1–55.
Weingarten, V.I., Seide, P., Peterson, J.P., 1968. Buckling of Thin-Walled Circular Cylinders. Special Publication NASA SP-8007. NASA.
Zoelly, R., 1915. Ueber ein Knickungsproblem an der Kugelschale. Buchdr. Zürcher & Furrer.